THE JOURNAL OF PHYSICAL CHEMISTRY C

Article

pubs.acs.org/JPCC

Quantum Confined Stark Effect in Au_8 and Au_{25} Nanoclusters

Xiaoming Wen,*[,†,§] Pyng Yu,[†] Yon-Rui Toh,[†] and Jau Tang*[,†,‡]

[†]Research Center for Applied Sciences, Academia Sinica, Taipei, Taiwan

[‡]Institute of Photonics, National Chiao-Tung University, Hsinchu, Taiwan

ABSTRACT: The quantum confined Stark effect is investigated for the first time in bovine serum albumin (BSA) protected Au_8 and Au_{25} nanoclusters. We observed a red-shift of 63 meV in Au_8 nanoclusters upon an increase in pH from 2.14 to 12.0. Such behavior could be well explained in terms of the presence of a linear polar component and a quadratic polarizable component. In contrast, Au_{25} nanoclusters exhibit more complicated Stark shifts due to their specific core/semiring structure. A plateau of the Stark shift was observed in both absorption and fluorescence, showing an offset of 30 meV. The lifetime measurements confirm that the plateau is due to the screening effect of the semirings in Au_{25}@BSA. Moreover, the dual fluorescent bands of Au_{25} nanoclusters exhibit two different Stark shifts of 79 and 52 meV, respectively. The experimental data indicate that the Stark shift in both Au_8@BSA and Au_{25}@BSA has a significant linear polar component due to their asymmetric structure. This study suggests that gold nanoclusters can become a potentially useful candidate in probing local electric fields and also in pH-sensing in nanoscale environment of biological systems.

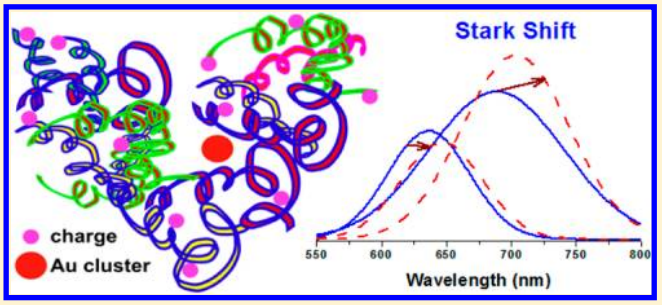

INTRODUCTION

Quantum-sized gold nanoclusters (NCs) have attracted enormous research interest due to their unique electronic and optical properties as well as a wide range of potential applications, including catalysis, biosensing, photonics, and molecular electronics.[1−6] Atomically precise gold NCs, when their sizes become comparable to the Fermi wavelength, exhibit unusual optical and electronic properties, such as discrete energy levels and vanished surface plasmon resonance.[7−9] It has been shown that gold NCs are nontoxic and highly photostable and thus very suitable for applications in monitoring biological processes.[10,11] In particular, gold NCs can be directly introduced into cell nucleus due to their ultrasmall sizes and functionalized ligands.[12,13] This unique feature provides a potential approach for nanoscale biosensing and drug delivery directly to the cell nucleus. Better physical understanding of the interaction between gold NCs and proteins is of critical importance for the development of nanoscale probes based on gold NCs.

The quantum confined Stark effect (QCSE) appears when an electric field is applied on a system in which the charged carriers are confined in one or more directions, resulting from a direct electric field or a local electric field induced by charges.[14−17] The QCSE has been extensively studied in semiconductor quantum wells and quantum dots (QDs) due to the potential applications in photonics.[16,18,19,23−25] Because of enhanced quantum confinement, gold NCs exhibit molecular highest occupied molecular orbital (HOMO)−lowest unoccupied molecular orbital (LUMO) in absorption and photoluminescence (PL). The internal Stark effect was investigated in biological system induced by charges.[20] It is expected that the Stark effect would appears in the emission and absorption when an electric field is applied on the electron−hole pairs in gold NCs. Bovine serum albumin (BSA) is one of the most abundant proteins in blood circulatory systems.[21,22] It is constituted by 585 amine acid residues, including 35 cysteines, which confers a relatively strong stability to the protein.[21,22] BSA-protected gold NCs have been shown to be highly luminescent with excellent photostability, biocompatibility, and nontoxicity, offering great potential applications in biosensing, bioimaging, and drug delivery involving single cells.[1,2,23,24] The conjugation of protein with NCs affords stabilization to the system. But more importantly, it also introduces biocompatible functionalities into these NCs for further biological interactions or couplings.[25,26] BSA is found to adopt a more flexible conformational state on the boundary surface of gold NCs as a result of the conformational changes in the bioconjugation. One of the advantages of BSA-protected NCs is that they can be suitable for a broad biologic environment from being extremely acidic to alkali.[27,28] How the electric field influences the optical properties in gold NCs is critically important for both fundamental understanding and practical applications.

Despite considerable theoretical and experimental efforts on gold NCs, fundamental understanding remains far from being complete. To date, the quantum confined Stark effect in gold NCs has not yet been studied. The study of QCSE could provide an insight for better physical understanding to facilitate their applications. In the present work, we investigate QCSE in

Received: November 27, 2012
Revised: January 24, 2013
Published: January 29, 2013

   dx.doi.org/10.1021/jp3116676 | J. Phys. Chem. C 2013, 117, 3621−3626

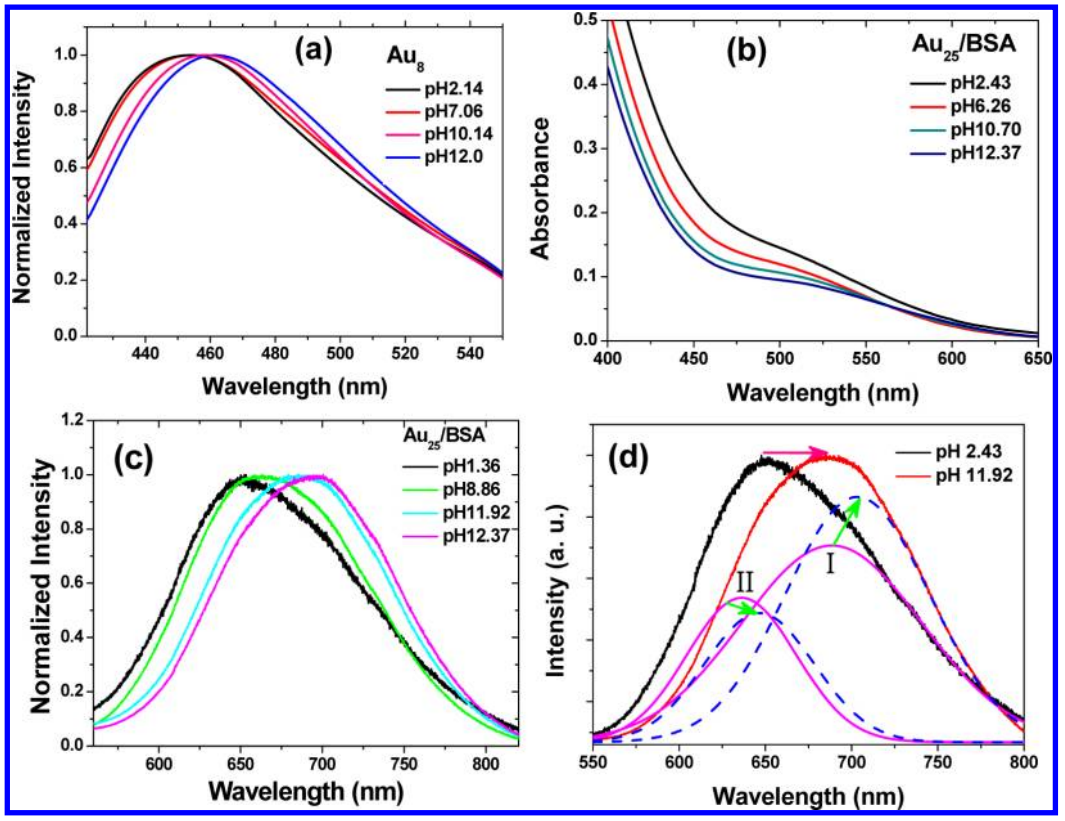

Figure 1. (a) Fluorescence spectra of Au_8@BSA as a function of the pH value. (b) Absorption and (c) fluorescence spectra of BSA-protected Au_{25} nanoclusters at various pH. An evident wavelength shift was observed when pH was changed. (d) The red-shift of Au_{25}@BSA of the dual Gaussian components from (black) pH 2.43 to (red) pH 11.92. With increasing pH, each Gaussian band exhibits an obvious red-shift and the bandwidth varies as well. The arrows indicate the corresponding Stark shifts of the PL band, band I, and band II, respectively.

BSA-protected gold NCs induced by a local electrical field controlled by pH. An evident Stark shift was observed in Au_8 NCs upon increasing pH, and it can be well described as a linear polar term and a quadratic polarizable term of the electric field. In contrast, Au_{25} NCs exhibit a more complicated Stark shift of absorption and fluorescence, owing to their specific core/semiring structure. Moreover, the dual fluorescent bands of Au_{25} NCs exhibit a different Stark shift correlated to their PL origins.[9] The presence of a significant linear polar component in the Stark shift suggests that both Au_8@BSA and Au_{25}@BSA have an asymmetric structure.

EXPERIMENTAL METHODS

Material Synthesis. The gold NCs used in this study were synthesized using a biomineralized approach.[9,29] Typically, 5 mL of 10 mM $HAuCl_4$ was mixed with 5 mL of 50 mg/mL BSA and kept at 37 °C overnight in an incubator while the pH was 8 and 11 for Au_8 and Au_{25}, respectively. It was found that the wavelength and PL spectrum exhibit good reversibility of pH. The fluorescence of pure BSA was compared at the identical concentration and conditions with that of Au_8@BSA. The autofluorescence from BSA can be safely excluded in the blue and green region because of the much weaker intensity in BSA.

Spectroscopic Measurements. In fluorescence measurements the solution sample was excited by a 406 nm CW laser and fluorescence was collected into a spectrometer (HORIBA Jobin Yvon) and recorded by a cooled CCD (Synapse CCD). The lifetimes were measured by the time-correlated single photon counting (TCSPC) technique on a Microtime-200 system (Picoquant) with excitation of a 467 nm laser. The absorption spectrum was measured in a spectrometer (JACOS).

RESULTS AND DISCUSSION

The BSA-protected Au_8 and Au_{25} NCs can be stabilized in a very broad range of pH, which is conducive for the biological applications.[30] As shown in Figure 1a, an evident red-shift of fluorescence was observed in Au_8 NCs upon increasing pH. It should be noted that the spectral shape of Au_8 NCs does not exhibit perceivable changes at various pH. Figure 1b shows the absorption spectra of Au_{25} NCs in which the characteristic absorption peak locates around 520 nm, similar to the other observation in BSA-protected Au_{25} NCs.[3,31] To analyze the variation of absorption peak at the different pH, the absorption spectrum was fitted by a Gaussian function.[32] Upon increasing pH the absorption of Au_{25} NCs exhibits an obvious red-shift that likely arises from the Stark effect, and the details will be discussed later. The fluorescent spectra exhibit an obvious red-shift with increasing pH, e.g., from 648 nm at pH 1.36 to 698 nm at pH 12.37 (Figure 1c). It should be emphasized that the fluorescence spectrum of Au_{25} NCs apparently varies other than shifts in wavelength upon changing pH. In the previous study it was demonstrated that the red fluorescence of BSA-protected Au_{25} NCs consists of two fluorescence bands that are closely correlated to the structure.[9] Band I at the lower energy dominantly originates from the icosahedral core, and band II mainly originates from the six -S-Au(I)-S-Au(I)-S- staples.[9] It should be noted that the fluorescence spectra at each pH can be well fitted by two Gaussian functions. We can separate the variations of two bands by fitting the fluorescence spectra at

dx.doi.org/10.1021/jp3116676 | J. Phys. Chem. C 2013, 117, 3621−3626

each pH using two Gaussian functions. Figure 1d is an example for the spectrum variation of bands I and II with pH changing from 2.43 to 11.92. It is distinct that both bands I and II display a red-shift upon increasing pH. Interestingly, the bandwidth and the intensity ratio between bands I and II vary at the same time.

It is well-known that the strength of the local electric field on a given point can be determined by the vector sum of the separate electric fields that each point charge would create in the absence of the others. Therefore, the strength of electric field on a Au NC can be expressed as $\mathbf{E} = \sum_{i=1}^{N}\mathbf{E}_i = 1/(4\pi\varepsilon)\sum_{i=1}^{N}(Q_i/r_i^2)\mathbf{r}_i = e/(4\pi\varepsilon)\sum_{i=1}^{N}(\mathbf{r}_i/r_i^2)$, where r_i is the position of charge and $\mathbf{r}_i$ is the corresponding unit vector. Therefore, the strength of electric field is determined by the charges in BSA and surrounding solvent as well as the charge distribution; it is also relevant to the relative position of Au NC in BSA. To date, calculation of the electric field in BSA is nontrivial and direct measurements of the electric field are still scarce, owing to the complicated, heterogenerous environment and frequently near solvated surfaces of irregular shape and composition.[20] pH-induced folding/unfolding and conformation variation with changing pH will also result in a variation of the strength of electric field.[33]

The pH-dependent conjugation between BSA and gold nanoparticles has been studied,[21,22,25,26,28,33] and BSA was suggested to own roughly a heart-shaped structure.[34] It was confirmed that the isoelectric point of the solution appears at pH 4.8.[21,35] Around this point the Au NC@BSA solution appeared to agglomerate due to denaturing of BSA.[22,33] At an even lower pH the agglomeration was dissolved while the PL intensity obviously decreases, most likely due to the increased defect states generated on the surface of the gold NCs. At a given pH, positive or negative charges could be induced in BSA as well as the interface between solvent and BSA, and thus a local electrical field is produced. Such an electric field can be controlled by tunning pH. Barbosa et al. studied the pH-induced conformational charges in BSA by the small-angle X-ray scattering (SAXAS) technique, and the charge number per BSA was determined at a series of given pH and roughly expressed by $N = 38.75 - 7.286(\mathrm{pH})$ according to the fitting.[21] The charge number per BSA can approximately represent the strength of electric field on Au NC due to the irregular distribution of Au NC in BSA[21,33] and the sign will represent the direction of the electric field. For a given pH, each gold NC will experience a local electric field due to the presence of charges in BSA and solvent. The charges in solvent are expected to have minor effect on Au NCs because the strength of electric field decreases rapidly with distance and BSA has a relative large size. As a consequence, the energy states of electrons and holes in gold NCs could be influenced by the electric field, and the corresponding spectra of absorption and fluorescence are expected to exhibit QCSE.[15,16]

Figure 2 shows the emission energy of fluorescence in Au_8 NCs as a function of the charge number per BSA. It has been shown that the discrete states of electron and hole in a quantum confined nanoparticle exhibit both polar and polarizable characteristics of the Stark effect under an external electric field.[14,15,19] QCSE has been observed by Bawendi et al. in single CdSe QDs under a direct current electric field,[15] and it was also observed under a local electric field induced by surrounding cations or anions.[17,20] The Stark effect may exhibit both polar and polarizable characters; namely, the excited

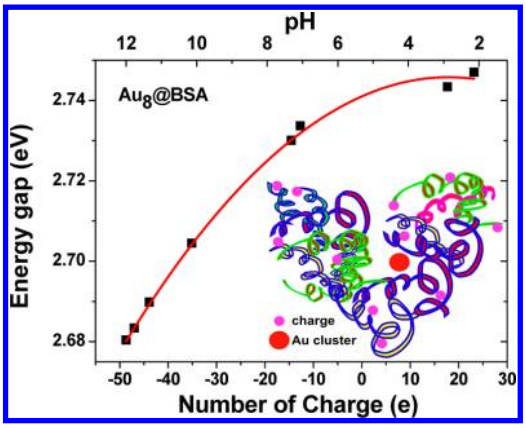

Figure 2. Emission energy of fluorescence as a function of charge number per BSA in Au_8@BSA NCs. The red line is the fitted curve according to eq 1. Inset schematically illustrates the gold nanocluster in a BSA.

energy shifts can be expressed as a linear polar term and a quadratic polarizable term of the electric field:[15]

$$\Delta E = E(F) - E(0) = -\mu F - \frac{1}{2}\alpha F^2 \quad (1)$$

where E is the energy of transition (absorption or emission), F is electric field strength, and μ and α are projections of the excited state dipole and polarizability along the electric field, respectively.[15] It is found that the emission energy of Au_8 NCs can be nicely fitted by eq 1, as shown the solid curve in Figure 2. The following parameters were extracted from the fit: $\mu = -(5.22 \pm 0.64) \times 10^{-4}$ meV/charge and $\alpha = (3.26 \pm 0.42) \times 10^{-5}$ meV/charge.[2] The geometry structure of Au_8 has been studied, yielding the structure of each Au_8 NC consisting of eight neutral Au(0) atoms.[29,36] Therefore, it is expected that no extra internal electronic field would influence the local field induced by the charges in BSA. In other words, the Stark shift results solely from the pH-induced local electric field. The fitting parameters indicate that Au_8 NC has an asymmetric structure because the linear dipole term is close to zero for a symmetric system and the Stark effect will become an even function of the electric field.[14,15] It was suggested that the most possible structures of Au_8 NCs are D_{2h} and C_{2v}.[37,38] C_{2v} is more likely the structure of Au_8 NCs.

Au_{25}@BSA has a very different structure. It has been shown that Au_{25} NC consists of an icosahedral core in which 12 Au(0) atoms form the vertices of the icosahedrons and enfold one central Au(0) atom. Then, six dimeric -S-Au(I)-S-Au(I)-S- staples form a semiring surrounding the core.[29,39,40] Pradeep et al. studied the evolution of Au_{25} NCs formation in BSA, and they confirmed that Au_{25} NCs form through a protein-bound Au(I) ion intermediate and subsequent emergence of free protein and Au(I)-S staple.[28] These staples are directly anchored to the surface via Au−S bonding, while the staples interact with the icosahedral core via Au−Au bonds.[8,41]

Figure 3 shows the Stark shifts for (a) absorption, (b) fluorescence of band I, and (c) fluorescence of band II as a function of the charge number per BSA in Au_{25} NCs. Upon increasing pH from 1.36 to 12.37, corresponding to a charge number of +30 to −50 per BSA, the absorption exhibits a shift of 48 meV, similar to the fluorescence of band II, 52 meV. In comparison, band I of Au_{25}@BSA exhibits a relatively larger shift of 79 meV. An evident difference with respect to the shift

dx.doi.org/10.1021/jp3116676 | J. Phys. Chem. C 2013, 117, 3621−3626

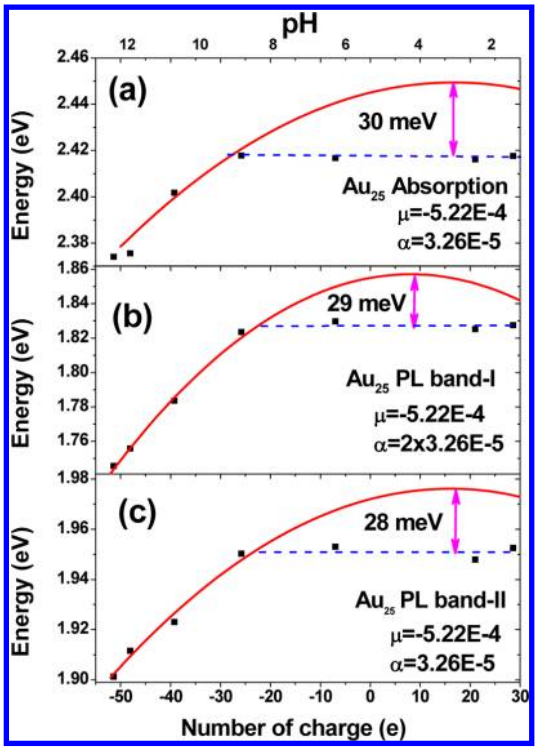

Figure 3. (a) Absorption peak, (b) fluorescence band I, and (c) fluorescence band II of Au_{25}@BSA as a function of the charge number per BSA. The dashed lines indicate the plateau, and the red curves represent the simulation with indicated parameters.

of Au_8 NCs is that a plateau of the Stark shift was observed for absorption and PL within a charge number of ±20. It can be ascribed to their different geometries and electronic structures. It should be emphasized that each Au_{25}@BSA consists of 13 Au(0) in icosahedral core surrounded by six -S-Au(I)-S-Au(I)-S- staples.[5,42] It is expected that the 12 Au(I) ions in the staples will induce an internal electronic field. Therefore, each Au_{25} NC will be influenced by both a local electric field induced by the charges distributed in BSA and an internal electric field induced by Au(I)s in the semirings. The semirings are spatially flexible, and thus they can deform to fit the local electric field when an electric field is applied. Upon increasing the charge number by changing the pH, the semirings can screen off the local electric field and keep the core at an unchanged electric field until the local field is beyond its screening capability.

Ritter and co-workers investigated the anomalous Stark effect induced by the lateral electric field on an electron−hole pair confined in a quantum dot.[14] They suggested that the Coulomb interaction between an electron and a hole can result in a plateau of the Stark shift when the lateral field is relatively weaker than the Coulomb interaction. Two competing effects of the electric field need to be taken into account. On one hand, the electric field is pushing the electrons and holes in opposite directions, which can lead to a decrease of excitonic oscillator strength. The lower one-particle energies of the carriers in their new positions give rise to a red-shift ($\alpha > 0$) of the excitonic line. On the other hand, the Coulomb interaction of an electron−hole pair is diminished by the separation of carriers; this will cause an increase in the potential energy of electron−hole pair and can result in a blue-shift.[14,43] In Au_{25}@BSA, the dipole moment and polarizability induced by the local electric field make contribution to QSCE. In addition, an extra electric field effect induced by Au(I) in the semiring needs to be taken into account. Upon increasing pH the charge number in a BSA increases and thus the local electric field will increase. The -S-Au(I)-S-Au(I)-S- staples can slightly deform and generate an extra internal electric field to resist the variation of the local electric field if the charge number is not too big. In this case, the net electric field on an Au_{25}@BSA can remain unchanged, equivalent to screening of the local electric field. With a further increase in the number of charges the local electric field becomes too strong so that the staples are not able to resist the change by deformation, corresponding to a significant Stark shift. It should be noted that the critical point appears at the same pH for absorption as well as bands I and II of fluorescence, as shown in Figure 3. We simulated the Stark shift of Au_{25}@BSA NCs by using the parameters extracted from Au_8 NCs, $\mu = -5.22 \times 10^{-4}$ and $\alpha = 3.26 \times 10^{-5}$. Interestingly, a good agreement was obtained in absorption and fluorescence of band II with the screening amount of 30 and 28 meV, respectively. However, such a simulation displays an evident deviation from the Stark shift in band I. We tried to simulate with a revised parameter $\alpha = 2 \times 3.26 \times 10^{-5}$, yet a better simulation was then obtained with a screening amount of 29 meV. It should be noted that band I exhibits an obvious larger Stark shift of 79 meV. Moreover, the simulation suggests that a larger Stark effect in band I arises from an increased contribution from polarizability; a significant linear component of polar moment in the Stark effect suggests that Au_{25}@BSA has an asymmetric structure both for the core and semiring.

There are two aspects for the mechanisms for the observed plateau in the Stark shift: the Coulomb interaction of the electron−hole pair and the screening effect by the semiring. It was confirmed that the variation of the Coulomb interaction induced by QCSE would result in the decrease of wave function overlapping of electrons and holes. As a consequence, the lifetime of electron−hole recombination obviously increased.[19,4445] To address the mechanism, we measured the lifetime of Au_{25}@BSA as a function of charge number by TCSPC techniques excited at 467 nm detected at 650 nm. The component of electron−hole recombination was extracted by two exponential fitting, as illustrated in Figure 4 showing the lifetimes as a function of charge number, corresponding to pH 1.39 to 12.43. It is clear that the variation of pH basically does not induce an evident variation of lifetimes. The largest lifetime appears at around the isoelectric point. Then, the lifetimes slightly decrease upon increasing the absolute charge number.

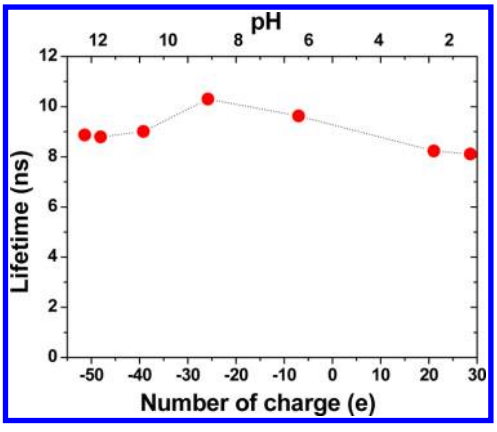

Figure 4. Recombination lifetime as a function of the charge number in Au_{25}@BSA.

dx.doi.org/10.1021/jp3116676 | J. Phys. Chem. C 2013, 117, 3621−3626

This result indicates that the recombination rate does not decrease with increasing local electric fields, and thus it confirms that the dominant mechanism for the plateau of the Stark shift is the screening effect by the semirings, rather than the Coulomb interaction of electron−hole pairs.

It is found that bands I and II reveal a complicated variation of bandwidth upon an increasing charge number, as shown in Figure 5. The bandwidths of bands I and II do not significantly

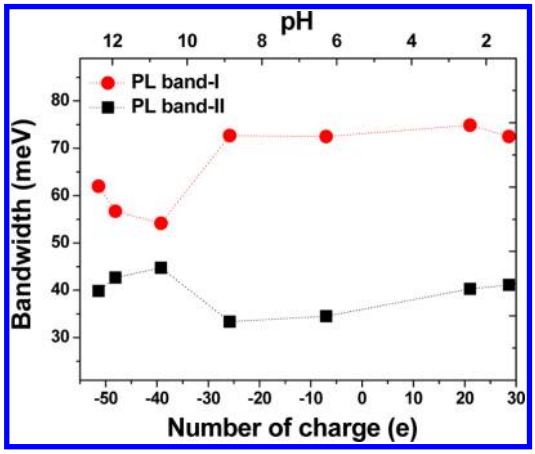

Figure 5. Bandwidths of band I (circles) and band II (squares) of Au_{25}@BSA as a function of the charge number.

change when the absolute charge number is less than 30, corresponding to the screening range of the semiring. When the charge number is larger than 30, the bandwidth of band I decreases significantly, from 75 to 55 meV. In contrast, the bandwidth of band II exhibits the opposite variation, from 35 to 45 meV.

In the previous study it has been shown that the spectral broadening in Au_8 and Au_{25} NCs is dominantly caused by the scattering of electron−electron and electron-ionized defects while the electron−phonon interaction has a minor contribution.[9,24] The bandwidths vary with the charge number should be relevant to the electron−electron interaction and electron-ionized surface/defect states. In particular, in the regime of a high charge number the bandwidths of the bands I and II exhibit the opposite variation, which suggests that the core and the semiring in Au_{25}@BSA experience different influences by the local electric field. To date, the detailed spatially distribution of Au NCs and charges in BSA is still a challenging work, although the geometric structure of a thoil monolater protected Au_{102} NCs was recently identified.[46] Further theoretical and experimental studies would be necessary for detailed understanding of the interactions between gold NCs and the charges in BSA.

CONCLUSION

We have investigated the quantum confined Stark effect in BSA-protected gold NCs. A local electric field could be established and varied in BSA by controlling its pH. A Stark shift of 63 meV was observed in Au_8 NCs, which is nicely fitted by the equation that takes account for both polar and polarizable effects. For Au_{25} NCs, both absorption and fluorescence spectra exhibit complicated Stark effects. An obvious plateau, about 30 meV, of the Stark shift appears at a lower charge number, for both positive and negative shifts. Lifetime measurements confirm that the plateau could be ascribed to the screening effect of the semiring by deformation. Moreover, the dual PL bands in Au_{25} NCs exhibit different Stark shifts. Band I exhibits a larger Stark shift, 79 meV, due to the larger polarizability contribution from the core. The significant linear polar component of the Stark shift indicates both Au_8 and Au_{25} NCs have an asymmetric structure. This study suggests that the ultrasmall sized gold NCs can become a potential candidate for probing electric fields or pH-sensing in the nanoscale of biological systems.

AUTHOR INFORMATION

Corresponding Author

*E-mail: x.wen@unsw.edu.au (X.W.); jautang@gate.sinica.edu.tw (J.T.).

Present Address

[§]ARC Photovoltaics Centre of Excellence, University of New South Wales, Sydney 2052, Australia.

Notes

The authors declare no competing financial interest.

ACKNOWLEDGMENTS

The authors acknowledge financial support from Academia Sinica (AS) Nano Program and National Science Council (NSC) of Taiwan under programs 99-2221-E-001-002-MY3 and 99-2113-M-001-023-MY3.

REFERENCES

(1) Zheng, J.; Nicovich, P. R.; Dickson, R. M. Highly Fluorescent Noble Metal Quantum Dots. *Annu. Rev. Phys. Chem.* **2007**, *58*, 409−431.

(2) Tanaka, S.-I.; Miyazaki, J.; Tiwari, D. K.; Jin, T.; Inouye, Y. Fluorescent Platinum Nanoclusters: Synthesis, Purification, Characterization, and Application to Bioimaging. *Angew. Chem.* **2011**, *50*, 431−435.

(3) Wen, X.; Yu, P.; Toh, Y.-R.; Hsu, A.-C.; Lee, Y.-C.; Tang, J. Fluorescence Dynamics in BSA Protected Au_{25} Nanoclusters. *J. Phys. Chem. C* **2012**, *116*, 19032−19038.

(4) Rao, T. U. B.; Pradeep, T. Luminescent Ag(7) and Ag(8) Clusters by Interfacial Synthesis. *Angew. Chem.* **2010**, *49*, 3925−3929.

(5) Parker, J. F.; Fields-Zinna, C. A.; Murray, R. W. The Story of a Monodisperse Gold Nanoparticle: Au(25)L(18). *Acc. Chem. Res.* **2010**, *43*, 1289−1296.

(6) Jin, R. Quantum Sized, Thiolate-Protected Gold Nanoclusters. *Nanoscale* **2010**, *2*, 343−362.

(7) Zheng, J.; Zhang, C. W.; Dickson, R. M. Highly Fluorescent, Water-Soluble, Size-Tunable Gold Quantum Dots. *Phys. Rev. Lett.* **2004**, *93*, 077402.

(8) Zhu, M.; Aikens, C. M.; Hollander, F. J.; Schatz, G. C.; Jin, R. Correlating the Crystal Structure of a Thiol-Protected Au25 Cluster and Optical Properties. *J. Am. Chem. Soc.* **2008**, *130*, 5883−5885.

(9) Wen, X.; Yu, P.; Toh, Y.-R.; Tang, J. Structure-Correlated Dual Fluorescent Bands in BSA-Protected Au25 Nanoclusters. *J. Phys. Chem. C* **2012**, *116*, 11830−11836.

(10) Shang, L.; Doerlich, R. M.; Brandholt, S.; Schneider, R.; Trouillet, V.; Bruns, M.; Gerthsen, D.; Nienhaus, G. U. Facile Preparation of Water-Soluble Fluorescent Gold Nanoclusters for Cellular Imaging Applications. *Nanoscale* **2011**, *3*, 2009−2014.

(11) Shang, L.; Brandholt, S.; Stockmar, F.; Trouillet, V.; Bruns, M.; Nienhaus, G. U. Effect of Protein Adsorption on the Fluorescence of Ultrasmall Gold Nanoclusters. *Small* **2012**, *5*, 661−665.

(12) Wang, Y.; Chen, J.; Irudayaraj, J. Nuclear Targeting Dynamics of Gold Nanoclusters for Enhanced Therapy of HER2+ Breast Cancer. *ACS Nano* **2011**, *5*, 9718−9725.

(13) Wang, Y.; Cui, Y.; Zhao, Y.; Liu, R.; Sun, Z.; Li, W.; Gao, X. Bifunctional Peptides That Precisely Biomineralize Au Clusters and Specifically Stain Cell Nuclei. *Chem. Commun.* **2012**, *48*, 871−873.

(14) Ritter, S.; Gartner, P.; Baer, N.; Jahnke, F. Anomalous Stark Effect in Semiconductor Quantum Dots. *Phys. Rev. B* **2007**, *76*, 165302.
(15) Empedocles, S.; Bawendi, M. Quantum-Confined Stark Effect in Single CdSe Nanocrystallite Quantum Dots. *Science* **1997**, *278*, 2114.
(16) Je, K. C.; Ju, H.; Treguer, M.; Cardinal, T.; Park, S. H. Local Field-Induced Optical Properties of Ag-Coated CdS Quantum Dots. *Opt. Express* **2006**, *14*, 7994−8000.
(17) Wang, W.; Liu, G.; Cho, H.; Guo, Y.; Shi, D.; Lian, J.; Ewing, R. Surface Charge Induced Stark Effect on Luminescence of Quantum Dots Conjugated on Functionalized Carbon Nanotubes. *Chem. Phys. Lett.* **2009**, *469*, 149−152.
(18) Kuo, Y. H.; Lee, Y. K.; Ge, Y.; Ren, S.; Roth, J. E.; Kamins, T. I.; Miller, D. A. B.; Harris, J. S. Strong Quantum-Confined Stark Effect in Germanium Quantum-Well Structures on Silicon. *Nature* **2005**, *437*, 1334−1336.
(19) Jarjour, A. F.; Oliver, R. A.; Tahraoui, A.; Kappers, M. J.; Humphreys, C. J.; Taylor, R. A. Control of the Oscillator Strength of the Exciton in a Single InGaN-GaN Quantum Dot. *Phys. Rev. Lett.* **2007**, *99*, 197403.
(20) Lockhart, D. J.; Kim, P. S. Internal Stark Effect Measurement of the Electric Field at the Amino Terminus of an Alpha Helix. *Science* **1992**, *257*, 947−951.
(21) Barbosa, L. R. S.; Ortore, M. G.; Spinozzi, F.; Mariani, P.; Bernstorff, S.; Itri, R. The Importance of Protein-Protein Interactions on the pH-Induced Conformational Changes of Bovine Serum Albumin: a Small-Angle X-ray Scattering Study. *Biophys. J.* **2010**, *98*, 147−157.
(22) Tsai, D. H.; DelRio, F. W.; Keene, A. M.; Tyner, K. M.; MacCuspie, R. I.; Cho, T. J.; Zachariah, M. R.; Hackley, V. A. Adsorption and Conformation of Serum Albumin Protein on Gold Nanoparticles Investigated Using Dimensional Measurements and in Situ Spectroscopic Methods. *Langmuir* **2011**, *27*, 2464−2477.
(23) Liu, C. J.; Zhang, P.; Tian, F.; Li, W. C.; Li, F.; Liu, W. G. One-Step Synthesis of Surface Passivated Carbon Nanodots by Microwave Assisted Pyrolysis for Enhanced Multicolor Photoluminescence and Bioimaging. *J. Mater. Chem.* **2011**, *21*, 13163−13167.
(24) Yu, P.; Wen, X.; Toh, Y. R.; Tang, J. Temperature Dependent Fluorescence in Au_{10} Nanoclusters. *J. Phys. Chem. C* **2012**, *116*, 6567−6571.
(25) Khullar, P.; Singh, V.; Mahal, A.; Dave, P. N.; Thakur, S.; Kaur, G.; Singh, J.; Kamboj, S. S.; Bakshi, M. S. Bovine Serum Albumin Bioconjugated Gold Nanoparticles: Synthesis, Hemolysis, and Cytotoxicity toward Cancer Cell Lines. *J. Phys. Chem. C* **2012**, *116*, 8834−8843.
(26) Shi, X. J.; Li, D.; Xie, J.; Wang, S.; Wu, Z. Q.; Chen, H. Spectroscopic Investigation of the Interactions between Gold Nanoparticles and Bovine Serum Albumin. *Chin. Sci. Bull.* **2012**, *57*, 1109−1115.
(27) Brewer, S. H.; Glomm, W. R.; Johnson, M. C.; Magne, K.; Franzen, S. Probing BSA Binding to Citrate-Coated Gold Nanoparticles and Surfaces. *Langmuir* **2005**, *21*, 9303−9307.
(28) Chaudhari, K.; Lourdu Xavier, P.; Pradeep, T. Understanding the Evolution of Luminescent Gold Quantum Clusters in Protein Templates. *ACS Nano* **2011**, *5*, 8816−8827.
(29) Le Guevel, X.; Hoetzer, B.; Jung, G.; Hollemeyer, K.; Trouillet, V.; Schneider, M. Formation of Fluorescent Metal (Au, Ag) Nanoclusters Capped in Bovine Serum Albumin Followed by Fluorescence and Spectroscopy. *J. Phys. Chem. C* **2011**, *115*, 10955−10963.
(30) Retnakumari, A.; Setua, S.; Menon, D.; Ravindran, P.; Muhammed, H.; Pradeep, T.; Nair, S.; Koyakutty, M. Molecular-Receptor-Specific, Non-Toxic, Near-Infrared-Emitting Au Cluster-Protein Nanoconjugates for Targeted Cancer Imaging. *Nanotechnology* **2010**, *21*, 005103.
(31) Xie, J.; Zheng, Y.; Ying, J. Y. Protein-Directed Synthesis of Highly Fluorescent Gold Nanoclusters. *J. Am. Chem. Soc.* **2009**, *131*, 888−889.
(32) Yaacobi-Gross, N.; Soreni-Harari, M.; Zimin, M.; Kababya, S.; Schmidt, A.; Tessler, N. Molecular Control of Quantum-Dot Internal Electric Field and Its Application to CdSe-Based Solar Cells. *Nat. Mater.* **2011**, *10*, 974−979.
(33) Shang, L.; Wang, Y.; Jiang, J.; Dong, S. pH-Dependent Protein Conformational Changes in Albumin: Gold Nanoparticle Bioconjugates: a Spectroscopic Study. *Langmuir* **2007**, *23*, 2714−2721.
(34) Sen, T.; Mandal, S.; Haldar, S.; Chattopadhyay, K.; Patra, A. Interaction of Gold Nanoparticle with Human Serum Albumin (HSA) Protein Using Surface Energy Transfer. *J. Phys. Chem. C* **2011**.
(35) Ao, L. M.; Gao, F.; Pan, B. F.; Cui, D. X.; Gu, H. C. Interaction between Gold Nanoparticles and Bovine Serum Albumin or Sheep Antirabbit Immunoglobulin G. *Chin. J. Chem.* **2006**, *24*, 253−256.
(36) Jain, P. K. A DFT-Based Study of the Low-Energy Electronic Structures and Properties of Small Gold Clusters. *Struct. Chem.* **2005**, *16*, 421−426.
(37) Lecoultre, S.; Rydlo, A.; Félix, C.; Buttet, J.; Gilb, S.; Harbich, W. UV−Visible Absorption of Small Gold Clusters in Neon: Au_n (n = 1−5 and 7−9). *J. Chem. Phys.* **2011**, *134*, 074302−8.
(38) Olson, R. M.; Gordon, M. S. Isomers of Au_8. *J. Chem. Phys.* **2007**, *126*, 214310−214310−6.
(39) Heaven, M. W.; Dass, A.; White, P. S.; Holt, K. M.; Murray, R. W. Crystal Structure of the Gold Nanoparticle $N(C_8H_{17})(4)$ $Au_{25}(SCH_2CH_2Ph)(18)$. *J. Am. Chem. Soc.* **2008**, *130*, 3754−3755.
(40) Akola, J.; Walter, M.; Whetten, R. L.; Hakkinen, H.; Gronbeck, H. On the Structure of Thiolate-Protected Au_{25}. *J. Am. Chem. Soc.* **2008**, *130*, 3756−3757.
(41) MacDonald, M. A.; Chevrier, D. M.; Zhang, P.; Qian, H.; Jin, R. The Structure and Bonding of Au(25)(SR)(18) Nanoclusters from EXAFS: The Interplay of Metallic and Molecular Behavior. *J. Phys. Chem. C* **2011**, *115*, 15282−15287.
(42) Wu, Z.; Jin, R. On the Ligand's Role in the Fluorescence of Gold Nanoclusters. *Nano Lett.* **2010**, *10*, 2568−2573.
(43) Heller, W.; Bockelmann, U.; Abstreiter, G. Electric-Field Effects on Excitons in Quantum Dots. *Phys. Rev. B* **1998**, *57*, 6270.
(44) Polland, H. J.; Schultheis, L.; Kuhl, J.; Göbel, E.; Tu, C. Lifetime Enhancement of Two-Dimensional Excitons by the Quantum-Confined Stark Effect. *Phys. Rev. Lett.* **1985**, *55*, 2610−2613.
(45) Wen, G.; Lin, J.; Jiang, H.; Chen, Z. Quantum-Confined Stark Effects in Semiconductor Quantum Dots. *Phys. Rev. B* **1995**, *52*, 5913.
(46) Jadzinsky, P. D.; Calero, G.; Ackerson, C. J.; Bushnell, D. A.; Kornberg, R. D. Structure of a Thiol Monolayer-Protected Gold Nanoparticle at 1.1 Å Resolution. *Science* **2007**, *318*, 430−433.